Supplementary Information for

Stoner Instability-mediated Large Magnetoelectric Effects in 2D Stacking Electrides

Zhigang Gui,[1] Haiyan Zhu,[1] Zhe Wang,[1] M. Umar Farooq,[1] Laurent Bellaiche[2], Li Huang[1,3*]

[1]*Department of Physics & Academy for Advanced Interdisciplinary Studies, Southern University of Science & Technology, Shenzhen, Guangdong, 518055, China*

[2]*Physics Department and Institute for Nanoscience and Engineering, University of Arkansas, Fayetteville 72701, USA*

[3]*Quantum Science Center of Guangdong-Hong Kong-Macao Greater Bay Area (Guangdong), Shenzhen 518045, China*

*E-mail: huangl@sustech.edu.cn

Supplementary Table 1. Properties (electric polarization, switching barrier and net magnetic moment) of polar stacking bilayer Hf_2S dependence on the Hubbard U value of Hf 5d electrons. The exact Hubbard U correction is expected to be not large for Hf 5d electrons since they are quite dispersive.

U (eV)	0.0	0.5	1.0	3.0	5.0
Polarization (pC/m)	2.38	2.06	1.39	1.05	0.61
Barrier (meV/f.u.)	125.11	104.33	101.20	102.39	198.88
Net magnetic moment (μ_B/u.c.)	0.35	0.35	0.13	0.08	0.06

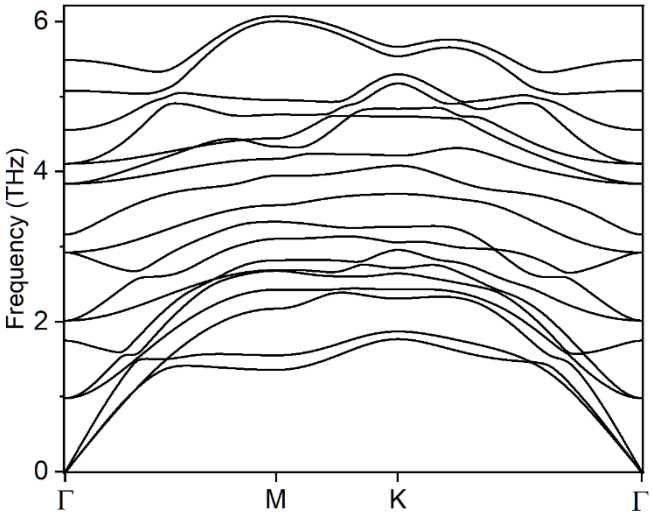

Supplementary Figure 1. Phonon dispersion of the polar stacking bilayer Hf_2S, which is calculated with density functional perturbation theory (DFPT) method[1] implemented in the Phonopy package[2, 3] with a supercell of $3 \times 3 \times 1$ size.

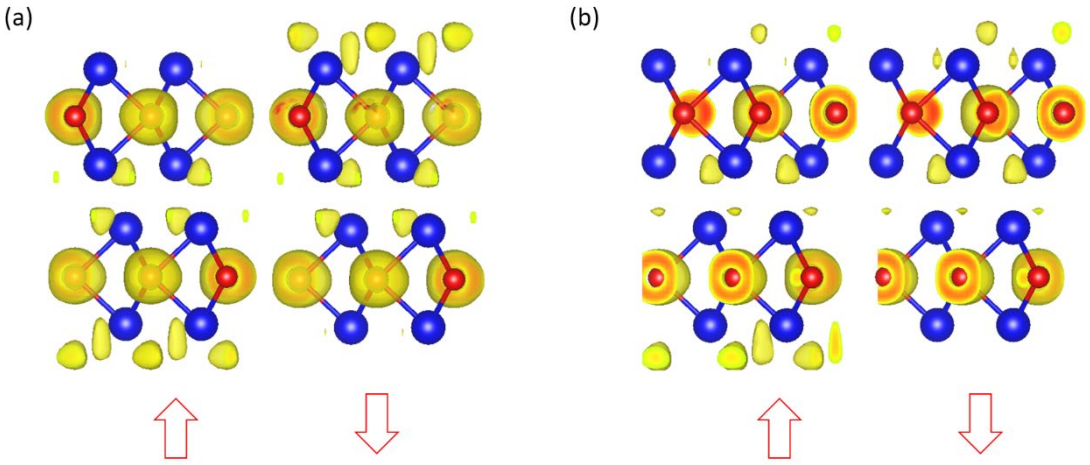

Supplementary Figure 2. Isosurface of electron localization function (ELF) for (a) the bulk stacking and (b) the polar stacking bilayer Hf_2S. The value of the isosurface is set to 0.5. The arrows indicate the spin channels. The position of the maximum of ELF in electrides may indicate the anionic electron center.

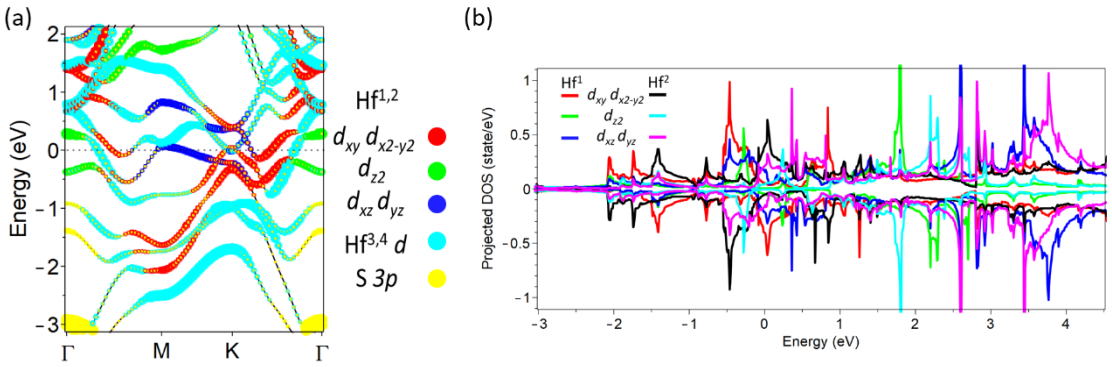

Supplementary Figure 3. Bulk stacking bilayer Hf_2S. (a) Atom-resolved electronic band structure (the spin-up and spin-down channel are equivalent and only one is shown). The radiuses of solid circles indicate the corresponding weights of the projections. (b) Projected density of states.

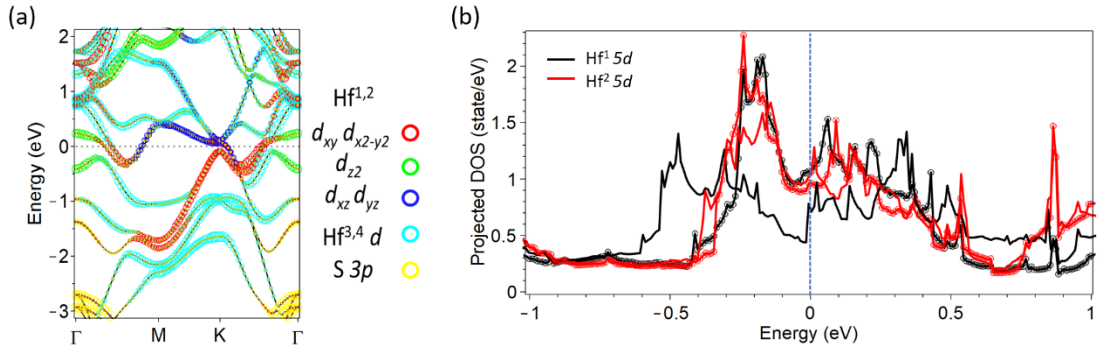

Supplementary Figure 4. Polar stacking bilayer Hf_2S (a) Atom-resolved electronic band structure for the nonmagnetic case. The radiuses of open circles indicate the corresponding weights of the projections. (b) Projected density of states for Hf^1 and Hf^2 located at the two opposite surfaces for the spin-polarized (solid line) and nonmagnetic (solid line + circle) cases. In the spin-polarized case, the sum of spin-up and spin-down component is shown.

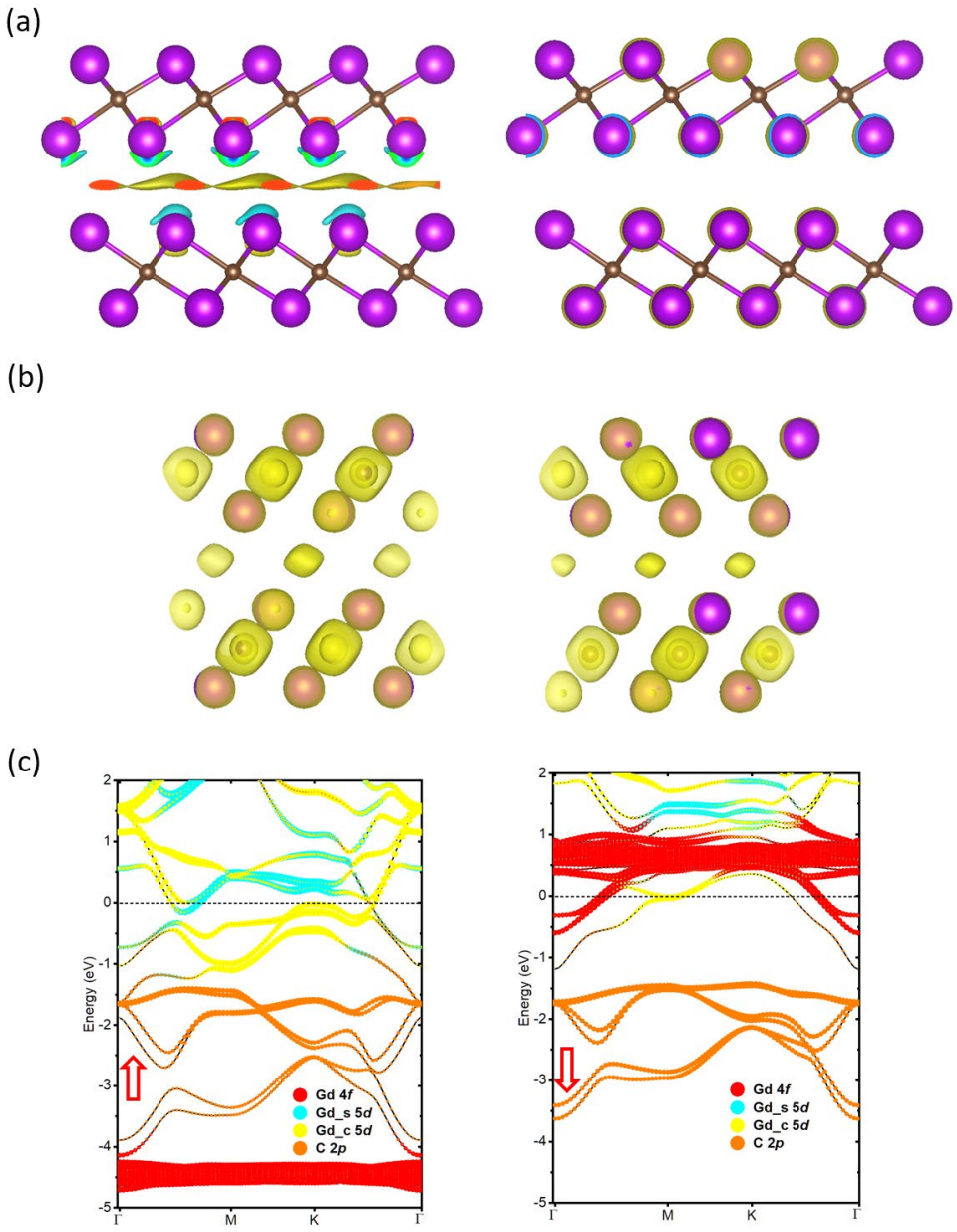

Supplementary Figure 5. Polar stacking bilayer Gd_2C. (a) Isosurface for differential charge density between the polar stacking bilayers and two single monolayers with the same atomic positions (left), and isosurface for the magnetization density (right). The values are set to 20% of the maxima. The positions of the interlayer anionic electron changes little along z direction and the dipole moment is around 0.004 eÅ/u.c. (b) the electron localization function (isosurface value set at 0.5) for bilayer bulk stacking (left) and polar stacking (right). (c) Atom-resolved electronic band structure for spin-up (left) and spin-down (right) channels.

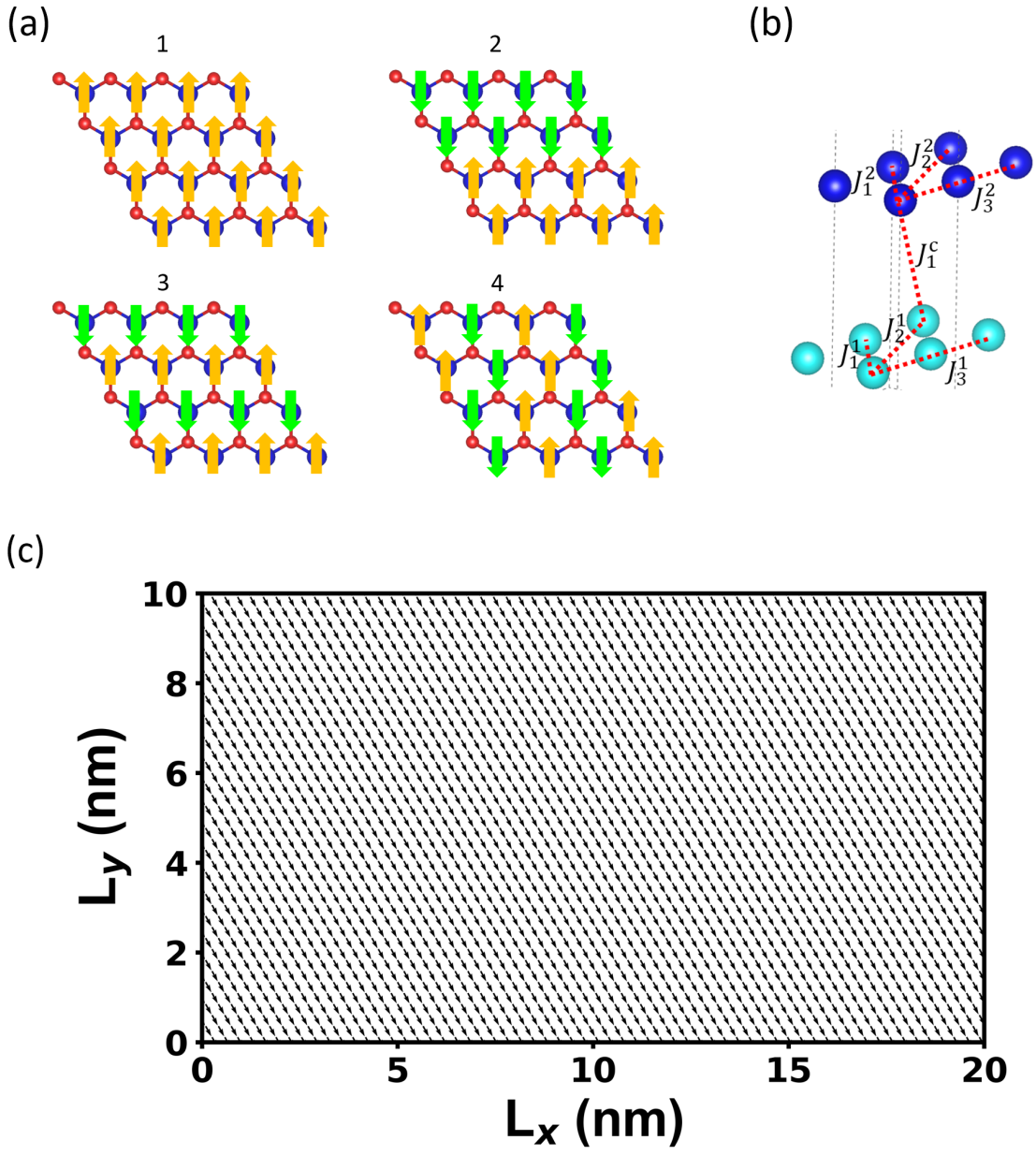

Supplementary Figure 6. Magnetic properties. (a) Configurations used to extract exchange parameters (only those of Hf^{1} atoms are shown here). (b) Exchange pairs of polar stacking bilayer Hf_2S. The spin Hamiltonian used here is given as

$$H = \sum_{p,\alpha,i,j} J_\alpha^p \vec{S}_i \cdot \vec{S}_j + \sum_{i,j} J_1^c \vec{S}_i \cdot \vec{S}_j + \sum_{p,i} A_i^p \left(\vec{S}_i^z\right)^2,$$

where $\alpha = 1,2,3$, representing the first, second and third nearest neighbors, $p = 1,2$, representing the two types of Hf atoms on the two opposite surfaces, J_1^c is the exchange parameter for the first nearest neighbors of two Hf atoms on different surfaces, A_i^p is the effective single-ion anisotropy from two different Hf atoms, and $\vec{S}_i^z$ is the z component of spin vector. Note that J_α^2 $(\alpha = 1,2,3)$ and J_1^c are comparably not as important as J_α^1 considering the small magnetic moments associated with them. Therefore, only J_α^1 are shown and used in the final calculations. We found that J_1^1=-128.74 meV, J_2^1 =53.16 meV, and J_3^1 =-39.98 meV. Negative values imply ferromagnetic couplings. With the inclusion of spin-orbit coupling, our calculations give an easy axis within the xy-plane, with a small magnetic anisotropy energy of 56 μeV/Hf, in contrast to the monolayer case which gives an easy axis along the out-of-plane direction. Note that the localized magnetic moment model adopted here to describe itinerant magnetism awaits further justification. (c) ferrimagnetic ground-state magnetic configuration confirmed by Monte Carlo simulation with the spin Hamiltonian above. $\vec{S}(= \vec{S}_{Hf^1} + \vec{S}_{Hf^2})$ is the total magnetic moment per unit cell and denoted by the arrows in the figure. The Monte Carlo simulation was conducted with the vampire package. 100000 steps are used for equilibrium and another 100000 steps are used for final statistics with cooling from 701K to 1K with a 5K temperature step.

Supplementary Table 2. The fitting parameters in Fig. 4(b) of the main text. C_{02} is fixed to 1.0. Other parameters such as C_{20} and C_{40} cannot be obtained from Fig. 4(b) alone. The unit is energy. Additionally, the slope of the linear fitting of the inset of Fig. 4b is -0.76.

Parameter	C_{12}	C_{22}	C_{11}	C_{21}	C_{31}
	-1.104	256.065	-8.394	-0.894	465.258

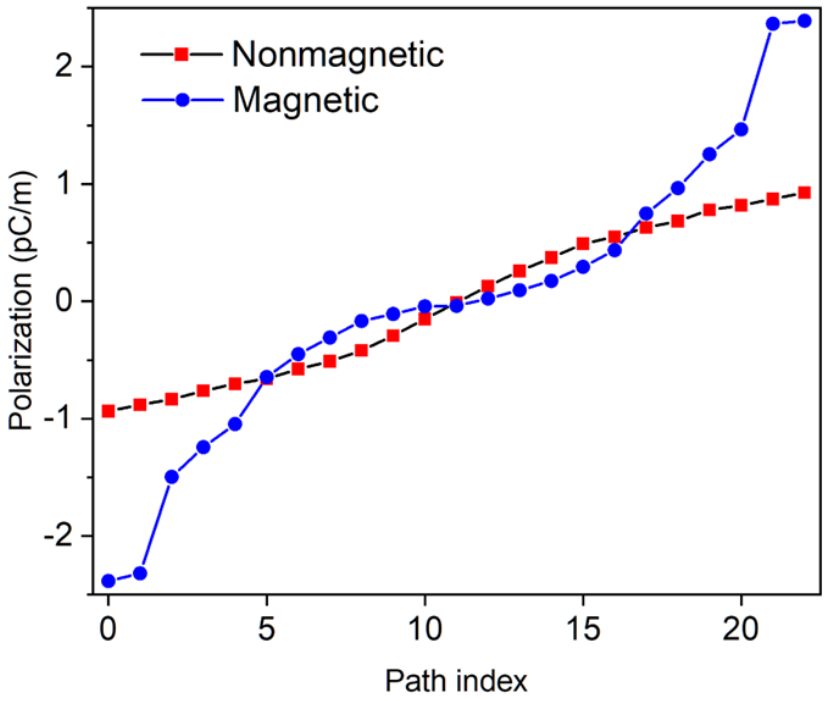

Supplementary Figure 7. The electric polarization of polar stacking bilayer Hf_2S along the switching path in the case of spin-polarized (blue dots) and nonmagnetic (red squares) calculations (lines are guide for the eye). The end points represent the degenerate ground states with the electric polarization pointing downward (Path index 0) and upward (Path index 22). If the polarization from nonmagnetic case can be deemed as solely from the distortion of electron cloud due to the polar stacking, then the difference of the polarization between nonmagnetic and magnetic cases can be thought as contributed from the magnetization. Accordingly, the polarization generated from the magnetization is 154% of that produced solely from the polar stacking, indicating a very strong magnetoelectric coupling.

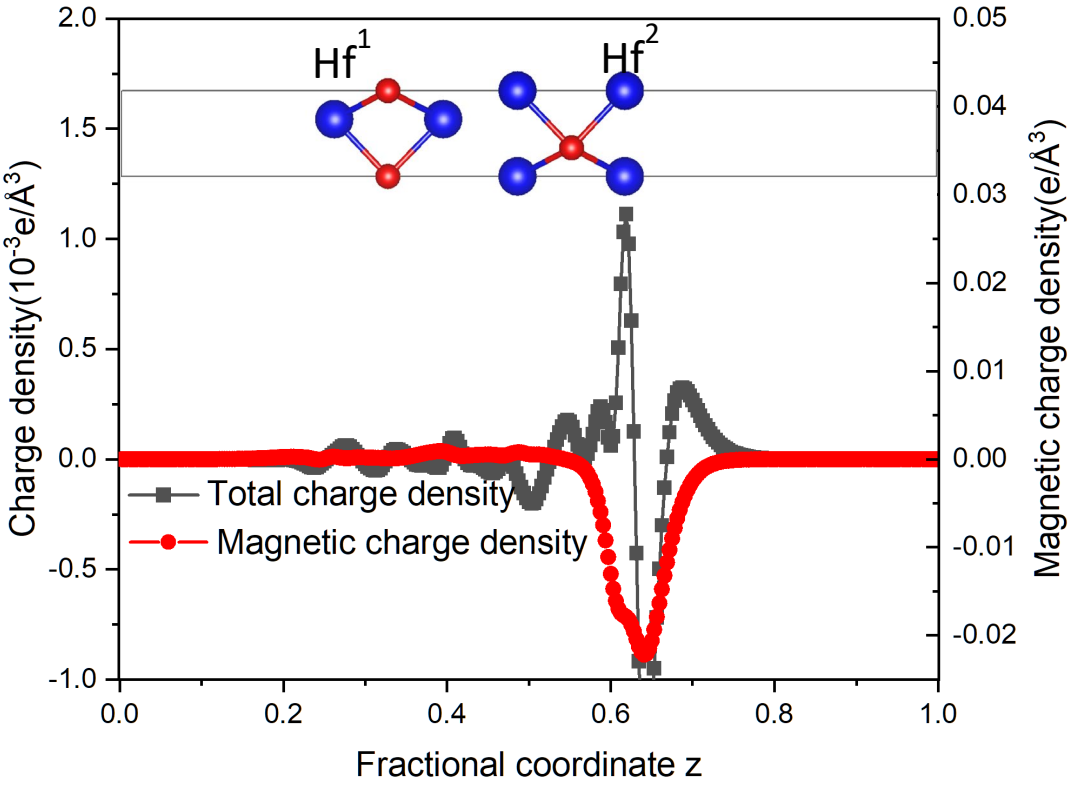

Supplementary Figure 8. The plane-averaged total charge (black squares) and magnetic charge (red circles) density difference between the structures from path index 0 and 2 in Fig. S7. The crystal structure along z direction is shown as a visual aid. Positive (negative) value means density accumulation (depletion). The deviation ΔQ (in Fig. 4(b) of the main text) is led by a discontinued increase of net magnetization and electric polarization, while the discontinued increase of net magnetization comes from the sharp decrease of the magnetic moments from Hf^2 as shown in the figure. As discussed in Fig. 2 of the main text, the decrease of the magnetic moment of Hf^2 is due to the weakening of the Stoner magnetism instability as a result of the reduction of projected density of states at the Fermi level of Hf^2 atom.

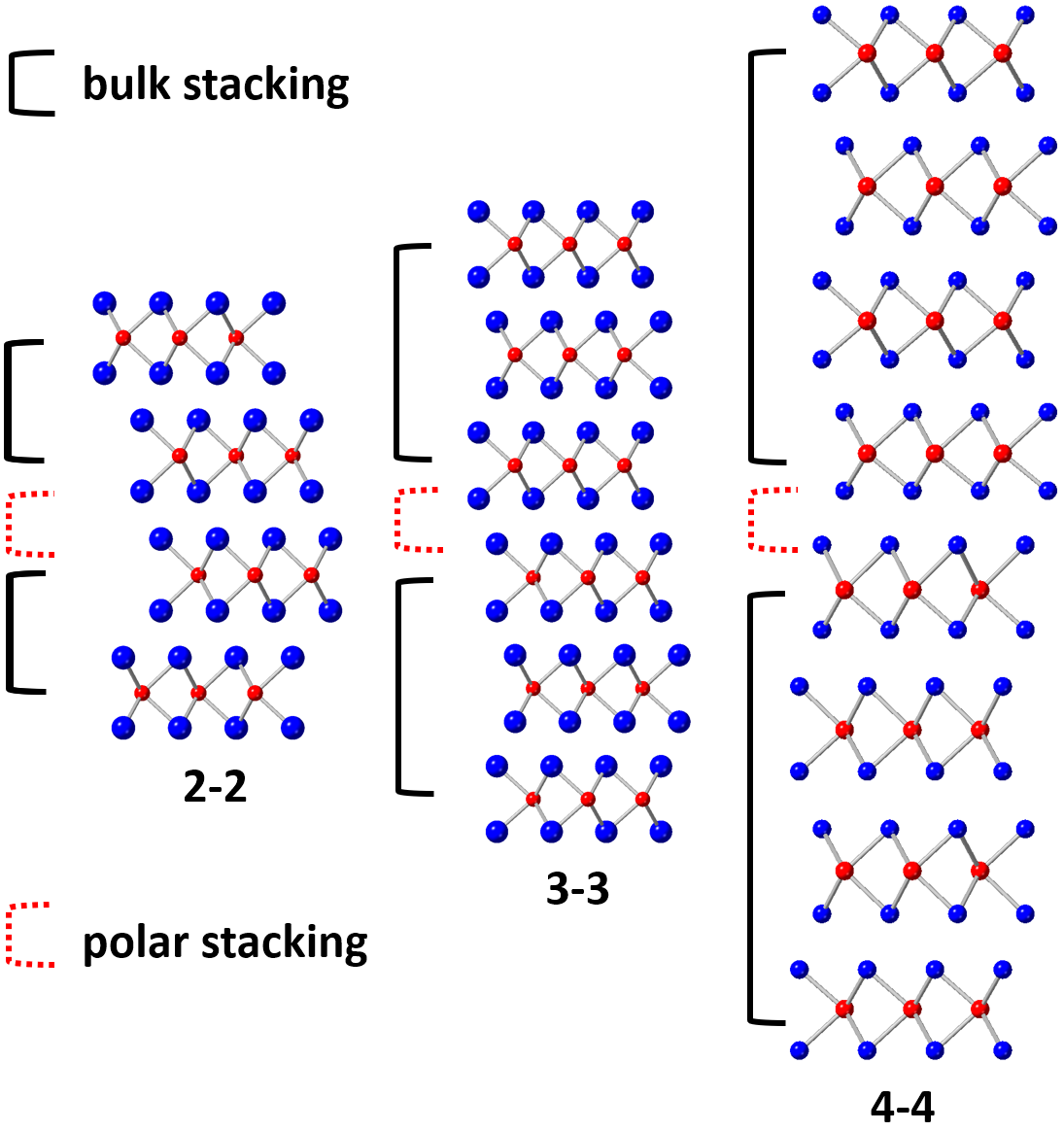

Supplementary Figure 9. Structures of the polar stacking of four, six and eight layers of Hf_2S. In each of them, stacking between the upper half and lower half of the structure remains polar, while stacking between adjacent layers within upper/lower half is kept to be similar to that of the bulk structure.

Supplementary Table 3. Properties (electric polarization, switching barrier and net magnetic moment) of the polar stacking of four, six and eight layers of Hf_2S.

Structure	1-1	2-2	3-3	4-4
Polarization (pC/m)	2.38	1.24	0.55	0.50
Barrier (meV/f.u.)	125.11	65.02	42.17	30.53
Net magnetic moment (μ_B/u.c.)	0.35	0.24	0.07	0.06

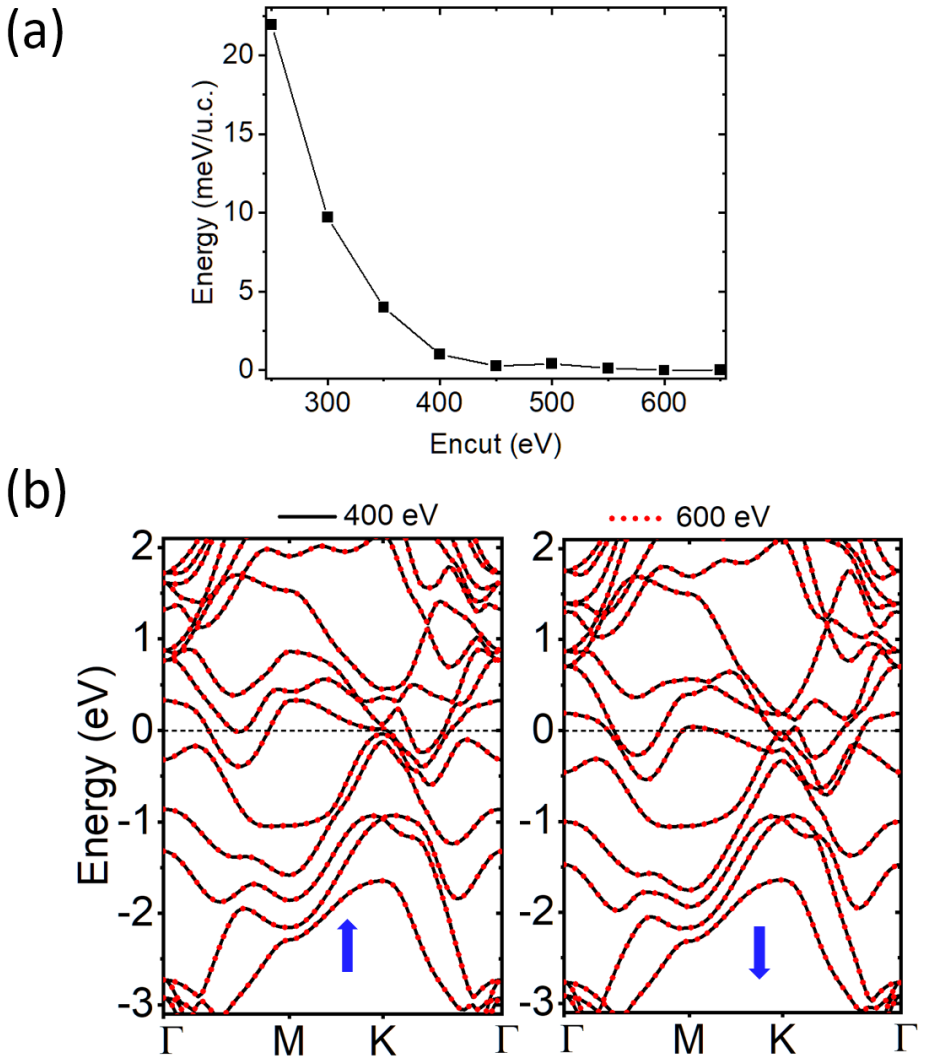

Supplementary Figure 10. Convergence with respect to the cutoff energy of plane wave basis used in the calculations for polar stacking bilayer Hf_2S. (a) relative energy of the ground-state structure of versus cutoff energy. (b) the spin polarized band structures calculated with cutoff energy of 400 eV (black solid line) and 600 eV (dots).

Supplementary References

(1) Gonze, X.; Lee, C. Dynamical matrices, Born effective charges, dielectric permittivity tensors, and interatomic force constants from density-functional perturbation theory. *Phys. Rev. B* **55**, 10355-10368 (1997).

(2) Togo, A.; Tanaka, I. First principles phonon calculations in materials science. *Scripta Mater.* **108**, 1-5 (2015).

(3) Togo, A.; Chaput, L.; Tadano, T.; Tanaka, I. Implementation strategies in phonopy and phono3py. *J. Phys.: Condens. Matter* **35**, 353001 (2023).